Plasma-catalyst interaction studied in a single pellet DBD reactor: dielectric constant effect on plasma dynamics

2017 Plasma Sources Sci. Technol. 26 065008

(http://iopscience.iop.org/0963-0252/26/6/065008)

OPEN ACCESS

Made open access 16 May 2017

IOP Publishing

Plasma Sources Science and Technology

Plasma Sources Sci. Technol. **26** (2017) 065008 (16pp)

https://doi.org/10.1088/1361-6595/aa6c35

Plasma-catalyst interaction studied in a single pellet DBD reactor: dielectric constant effect on plasma dynamics

T Butterworth[1,2] **and R W K Allen**[1]

[1] Department of Chemical and Biological Engineering, The University of Sheffield, United Kingdom
[2] Dutch Institute for Fundamental Energy Research (DIFFER), Eindhoven, The Netherlands

E-mail: t.d.butterworth@differ.nl

Received 18 October 2016, revised 27 March 2017
Accepted for publication 10 April 2017
Published 8 May 2017

Abstract

A novel single dielectric pellet DBD that is designed to facilitate studying the interaction between plasmas and catalysts is presented. The influence of material dielectric constant on plasma dynamics across a range of applied voltages is determined through the use of electrical characterisation combined with videos of the discharge. Different discharge modes in nitrogen are observed and their behaviour is characterised. A particular focus is given to the phenomenon known as 'partial discharging'. This is where incomplete plasma formation occurs between the electrodes of the reactor, which may have implications for the fair testing of catalysts in packed bed reactors. Additionally, the occurrence of an 'almond shaped' QV plot in the event of point-to-point discharging in PBRs is explained. This work provides easily implemented analytical techniques that can be applied to understand the behaviour of plasmas within packed bed DBD reactors.

Supplementary material for this article is available online

Keywords: plasma-catalysis, single pellet reactor, packed bed reactor, Lissajous plot, diagnostics

1. Introduction

Packed bed DBD reactors (PBRs) are promising for energy and environmental gas processing applications, as they combine the advantages of both catalysis and plasma technologies. The properties of the packing material have a dominant influence on the mechanism of plasma formation in the packed bed. The mechanism of plasma formation will change the electron properties in the plasma which will, in turn, change the chemistry. Hence, the efficacy of the plasma-catalytic reactor is linked to the co-dependency of the plasma discharge with the properties of the catalyst [1]. Consequently, identifying the influence of variables on experimental outcomes is inherently difficult. Furthermore, without having a theoretical framework, predicting how these variables will change experimental outcomes in untested operating conditions is extremely difficult. This presents a critical challenge to the future development of these reactors, particularly with scaling up reactors beyond bench scale. Techniques that help to develop a fundamental understanding of the plasma-catalyst interaction will therefore improve the rate of development of the technology.

The single catalyst pellet DBD reactor (SPR) presented in this work can be used for fundamental studies of plasma-catalyst interactions. It is envisaged that this reactor could be used with optical diagnostics, to validate computer models, and crucially—to understand the impact of packing material on plasma behaviour. In this work, the plasma behaviour is characterised using video (included with the supplementary information, available online at stacks.iop.org/PSST/26/065008/mmedia), combined with electrical characterisation via rapid analysis of QV plots (aka Lissajous figures) using LabVIEW. The SPR is demonstrated here by revisiting the influence of material dielectric constant on plasma behaviour.

High dielectric constant materials in PBRs are known to magnify local electric field strengths, and consequently reduce the onset voltage of electrical breakdown. However, the influence of dielectric constant on plasma discharge phenomena is

not well known. There are two identified mechanisms of plasma discharges in PBRs; streamer like surface discharges and point-to-point discharges [2, 3]. With increasing applied voltage to a PBR, plasma formation is believed to initially occur at the contact points between pellets, and subsequently transition to surface streamers at higher voltages [2]. The different discharge modes lead to changes in the distribution and extent of plasma formation throughout the reactors, as well as a likely change in electron energy distributions and densities. The electron properties in a plasma dictate the mechanism of plasma-chemical reactions, hence these two different discharge types may result in different chemistry occurring in the plasma. Additionally, catalyst activation by plasma is dependent on the location and mechanism of plasma formation in relation to the catalyst surface. This is due to the short lifetime of plasma activated species, which can be on the order of nanoseconds, meaning that some species have a mean free path as short as 60 μm [4]. However, it is currently unknown how plasma behaviour influences surface chemistry.

Previous research, predominantly by Kim *et al*, into discharge phenomena in PBRs have used photography [2, 3, 5], and electrical characterisation [3, 6, 7] to study randomly packed beds of various packing materials. These studies have revealed important features of both the point-to-point and surface discharges, and their relation to the resultant chemistry and plasma behaviour. In one example, surface conductivity, and consequently surface streamers, were found to have a strong influence on catalyst activity [5]. In another experiment, the so called 'memory effect' associated with DBDs, where streamers repetitively form in the same location on consecutive discharge cycles, does not occur with surface streamers in PBRs [2]. This fact, combined with the random location of packing, and the consequent non-uniformity in electric field means that optical studies of packing-discharge interactions would not be easily repeatable.

Spatial confinement of individual discharge filaments has been achieved in dielectric barrier discharges with very small ($\sim$1 mm) electrodes. This has facilitated a number of electrical and optical studies on a single DBD filament [8–11]. Similarly, studies of the electrical characteristics of multiple streamer discharges in DBDs have been achieved by limiting the electrode area such that only a small number of streamers can occur per discharge cycle [12–15]. To date, these studies have allowed the measurement of the spatial and temporal properties of the streamers, and their electrical characteristics in a range of gasses. Combined with modelling studies of these streamers, the dynamics of discharges in DBDs is relatively well understood. This has allowed the modelling of complex chemistry in individual streamers [16], and subsequently in more complex fluid models [17]. This approach of studying spatially constrained discharges with catalysts is untested. As it stands currently, modelling of discharges in PBRs is limited to simple chemistry sets in 3D geometries [18, 19], or more complex chemistry in 2D geometries [20]. The simple reactor geometry presented in this work should additionally help to validate the PBR models for more complex chemistry sets as they develop.

There are three major outcomes to the work presented here:

1. The different discharge modes, point-to-point discharges and surface streamers, are characterised.
2. The relationship between these different discharge modes and packing dielectric constant is determined.
3. Simple qualitative and quantitative methods to understand plasma behaviour based on *QV* plots are developed.

2. Experimental set-up

2.1. Reactor design

The reactor shown in figure 1 features five main components: a quartz glass reactor, two electrodes and two end plugs.

Reactor—The quartz glass reactor is a 50 mm long, 8 mm outer diameter, 6 mm inner diameter tube, with two ¼ inch gas ports located 12 mm from either end of the reactor. These two gas ports are connected to the external gas supply by push fit connectors. *Electrodes*—Both electrodes are made from a turned brass rod featuring an active electrode region, as well as a 35 mm long, 1.9 mm diameter interconnect to connect with the external circuit. The interconnect region is encased in a 0.5 mm thick alumina tube to prevent the formation of stray discharges. *Live electrode*—The live electrode active region has a diameter of 4 mm and a 1 mm thickness, with the plasma facing circumference of the electrode rounded to prevent formation of corona like discharges. The pellet to be tested sits in a 200 μm hemispherical indentation formed using a 3 mm diameter spherical tip drill bit centred in the end of the live electrode. The live electrode is centred in the reactor by a 5.8 mm diameter alumina 'collar' perforated with 150 μm holes around its circumference to allow gas flow through the reactor. The non-plasma forming end of the electrode is connected directly to an adapted PTFE high voltage connector (Genvolt TV-40) that provides a rigid and safe support for the whole reactor assembly. *Ground electrode*—The active region of the ground electrode is a 4 mm brass disk, with a 1 mm thickness encased inside an alumina dielectric. The dielectric layer is an adaptation of a commercially available crucible (Almath TGA 5.5). It is a 5 mm long cylinder with an outer diameter of 5.5 mm. The cylinder is closed at one end by a 0.5 mm thick wall that forms the dielectric layer. The brass electrode is sealed into the crucible using silicone sealant. Alumina based sealants were tested for this purpose but it was found that despite their favourable thermal and chemical resistance, they did not perform well as a dielectric and limited the performance of the reactor.

End plugs—The end plugs perform two tasks, to provide a gas seal to the atmosphere inside the reactor, and to centre the electrodes. The plugs are made from PEEK, and feature two silicone O-rings for gas seals. The inner O-ring compresses into the glass walls of the reactor, whilst the outer O-ring is compressed onto the electrode interconnect by a thumb screw.

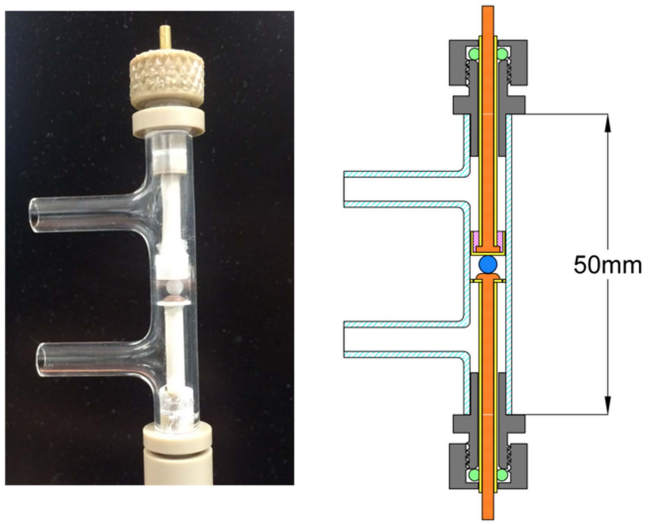

Figure 1. Photo and to scale schematic diagram of the single pellet reactor. The schematic is colour coded to show material components: brass (orange), glass (pale blue), alumina (yellow), PEEK (grey), pink (silicone sealant), green (silicone), test pellets (dark blue).

2.2. Description of apparatus

The reactor is driven by a Trek 10–40A/HS high voltage (HV) amplifier, giving voltage amplitudes up to 10 kV, at frequencies up to ~10 kHz. The signal to the amplifier is generated by a National Instruments DAQ-6211 controlled by a LabVIEW programme. Two electrical signals are monitored: the voltage output signal from the HV amplifier, and the charge transfer in the reactor obtained by measuring the voltage across a 4.7 nF 50 V X7R ceramic monitor capacitor. The gas is zero grade N_2 (BOC) at a fixed flowrate of 150 ml min^{-1}. The oscilloscope is a USB powered Picoscope 4224. A diagram of the experimental setup is presented in figure 2.

Photographs and videos of the plasma discharge around the pellet are taken with a Nikon D5300 with a 105 mm macro Lens (AF-S Micro Nikkor 105 mm 1:2.8G). The reactor is held in a fixed position relative to the camera using an aluminium support frame, with the head of a tripod camera mount affixed approximately 20 cm away. This gives the camera a lateral view of the reactor, with the catalyst pellet occupying the maximum area of the camera sensor whilst allowing the pellet to be in focus.

2.3. Material properties

Five different pellet materials are tested, each of them having a different dielectric constant. Each pellet is approximately spherical and has a diameter of 3 mm ± 0.1 mm, measured with a digital calliper. There are variations in the surface of roughness and porosity of each material, although this is not quantified. The yttria stabilized zirconia (YSZ—CoorsTek), $CaTiO_3$ (Catal International), $BaTiO_3$ (Catal International) and SiO_2 (Aigma Aldrich) are dense, with a very low porosity, whilst the Al_2O_3 (Sigma-Aldrich) used is highly porous. The dielectric constant of the $BaTiO_3$ has been experimentally tested using an LCR meter, and found to have a value of 4000 [21]. The other materials are assumed to take their values described in literature. These are shown in table 1.

2.4. Description of LabVIEW programme

A LabVIEW program simultaneously generates the signal to the reactor via the DAQ, and records data via the Picoscope. There are three main purposes to the programme:

(1) To very rapidly sweep through a range of applied voltages to the reactor so that gas heating in the reactor is minimal. Gas heating changes the behaviour of the discharge, and consequently prevents the fundamental property of interest (in this case dielectric constant) being studied independently of temperature change.
(2) To take the raw oscilloscope data and to cut it into individual discharge cycles that have a length of one period of the applied signal, i.e. multiple consecutive cycles of single shot data. These single shot data are then used in two ways; for analysis individually and to obtain an average Lissajous signal for each input voltage.
(3) To give accurate timings to the voltage increments applied to the reactor, meaning that events that take place in the reactor can be observed from the video data and compared with the applied signal.

The LabVIEW programme sweeps through a range of voltages with a fixed incremental step change in applied voltage. The desired purpose is to obtain and analyse as many Lissajous figures in as short a time frame as possible. This process is therefore limited by the speed and memory of the PC running the programme. The computer used in this experiment was capable of obtaining and analysing data from 40 sequential AC cycles every 0.7 s.

The typical settings used in this experiment sweep the source signal voltage from 0–10 V, in increments of 0.1 V. This signal is then amplified by 1000 times by the Trek power source. Using a step time of 0.7 s, with a total of 102 voltages tested, this gives a total run time per experiment of 71.4 s, in which ~4000 data points are obtained. The sample rate of the oscilloscope is 20 MS s^{-1}. At 0.2 s into each incremental change in voltage the oscilloscope data is sampled. The oscilloscope runs in 'block mode', transferring accumulated data from its data buffer to the PC in 'blocks' of data, with each sequential AC cycle sampled from one block of data.

2.5. Theory

The *Q–V* plots are commonly used for energy measurements of DBD and PBR reactors [22, 23], determination of gas gap charge transfer, reactor capacitances and burning voltage of the plasma in the reactor. Increasingly, they are used as a diagnostic method to quantify reactor performance in DBDs and PBRs. However, the relationship between *Q–V* plot characteristics and plasma behaviour in packed bed reactors is only partially defined.

In order to develop an understanding of plasma behaviour in PBRs, a comparison must be first made to DBDs.

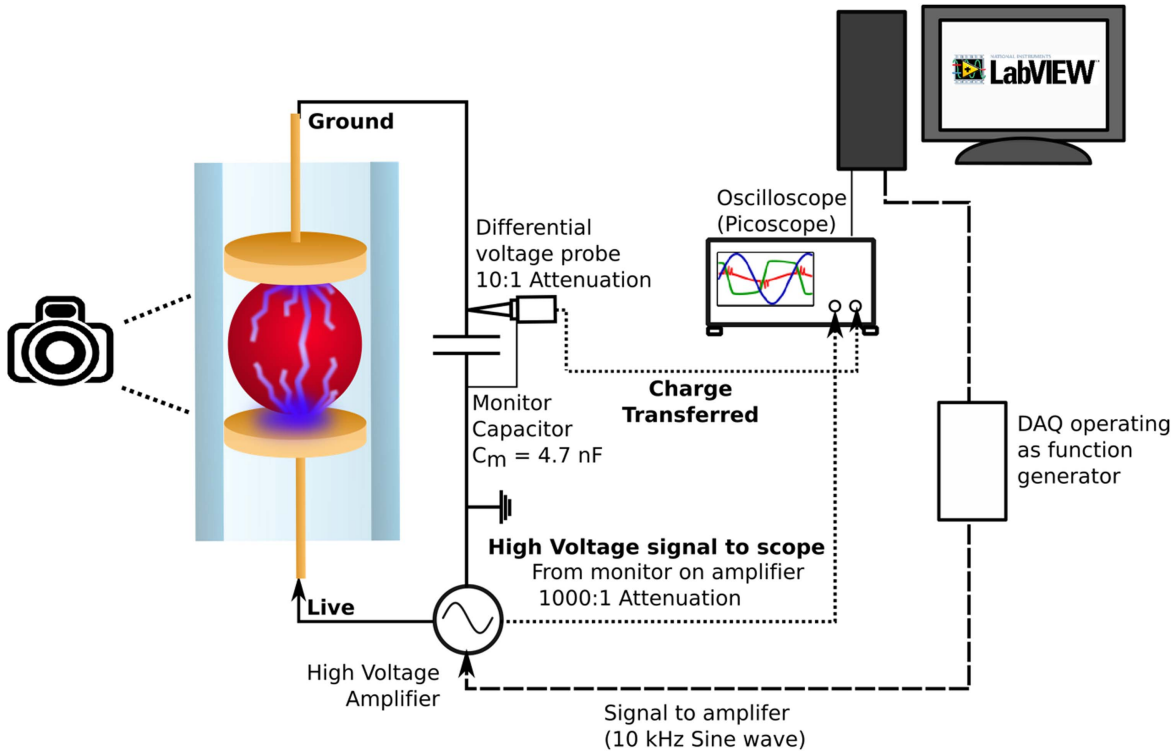

Figure 2. Experimental schematic depicting the voltage and charge monitor circuits.

Table 1. Dielectric constant of the pellets tested.

$BaTiO_3$	$CaTiO_3$	YSZ	Al_2O_3	SiO_2
4000	200–300	27	9–10	4

The classical equivalent circuit model for plasma discharges in DBDs is represented by two capacitors in series, with a resistor (or in some diagrams—two antiparallel Zener diodes) connected in parallel with one of the capacitors, as shown in figure 3. R_{plasma} represents the resistance of the plasma, and C_{diel} and C_{gap} are the capacitance of the dielectric layer and the gap respectively. Collectively, C_{diel} and C_{gap} give the overall cell capacitance, C_{cell}, by summation of the reciprocal of the capacitances (equation (1)).

$$\frac{1}{C_{cell}} = \frac{1}{C_{diel}} + \frac{1}{C_{gap}}. \quad (1)$$

In a typical DBD discharge, the Q–V plot appears as a parallelogram. The four sides of the parallelogram correspond with the discharging phases of a DBD in one period of the applied sinusoidal wave. The gradient of the Q–V plot line at any point is equal to the reactor capacitance at that instantaneous moment ($C = Q/V$).

There are two discharging phases (‘plasma on’—lines BC and DA), and two capacitive phases (‘plasma off’—lines AB and CD). During the capacitive phase, when no plasma is present, the reactor acts purely as a capacitor, having capacitance equal to C_{cell}. During the discharging phase, i.e. the time period that the gap voltage exceeds the threshold burning voltage, microdischarges transfer charge across the DBD gas gap. At this point, the discharge gap ceases to act as a capacitor and only the dielectric layer is capacitive, therefore the capacitance is equal to C_{diel}. The dielectric capacitance, C_{diel}, is solely determined by the geometry and the materials that the dielectric layer is fabricated from, consequently it has a fixed value (neglecting the effects of reactor temperature and applied signal frequency). This behaviour defines the ‘classical’ DBD equivalent circuit originally identified by Manley.

There are a number of possible deviations from the classic DBD equivalent circuit. Here, we briefly discuss three of these possibilities and their relation to this article:

(1) The partial discharging equivalent model of Peeters and van de Sanden (hereafter abbreviated to the Peeters model).
(2) The variable capacitance of plasma actuators as described by Kriegseis *et al.*
(3) The equivalent circuit model for PBRs, discussed in part by Mei *et al* and Tu *et al.*

The model of Peeters describes scenarios for DBDs in which an area of the electrodes is not discharging, this is termed ‘partial discharging’. Partial discharging occurs when the applied voltage amplitude is only marginally in excess of the reactor breakdown voltage. This phenomenon is identified when the calculated capacitance determined by the gradient of the discharging line (lines BC and DA in figure 3) is less than the actual dielectric capacitance. Peeters suggests that this measured capacitance, termed the ‘effective capacitance’ (ζ_{diel}), is linearly dependent on the area of the electrode discharging [24, 25]. As in the classic circuit, a discharging

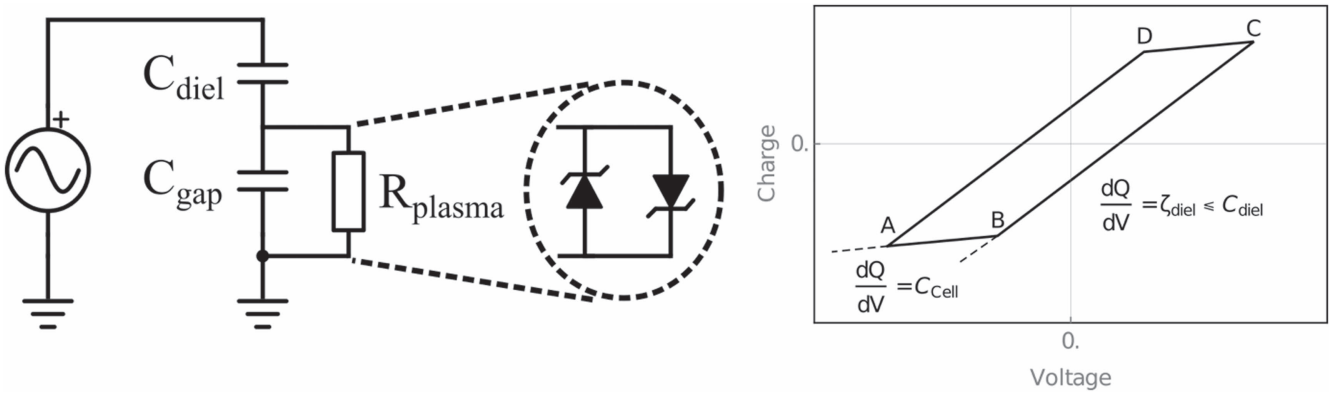

Figure 3. Classic equivalent circuit model for a DBD with corresponding ideal *QV* plot parallelogram.

electrode has capacitance, C_{diel}, and a non-discharging electrode, C_{cell}. However, in this case the discharging and non-discharging areas of the electrode collectively give the overall average capacitance measurement, ζ_{diel}. In the work of Peeters and van de Sanden, the *Q–V* plot presents as a classical DBD parallelogram, and hence the gradient of ζ_{diel} is only dependent on the applied voltage amplitude (as opposed to an instantaneous voltage, described later in this work).

The fractional area of the electrode that is not discharging, α, can be calculated by equation (2):

$$\alpha = \frac{C_{diel} - \zeta_{diel}}{C_{diel} - C_{cell}}, \tag{2}$$

where C_{diel} and C_{cell} are the geometrically determined reactor capacitances, and ζ_{diel} is the measured effective capacitance. This corresponding equivalent circuit model is shown in figure 4.

Kriegseis *et al* describe 'almond shaped' *Q–V* plots in plasma actuators, i.e. the capacitance varies as a function of the applied voltage. This is attributed to the growth of the plasma channel along the electrode during a discharge cycle. Hence, the instantaneous capacitance changes as a function of the plasma channel length, which in turn changes as a function of applied voltage. The same voltage dependent capacitance phenomenon is observed in this work, as well as in other PBRs [21]. Albeit, the plasma growth does not happen along the electrode but at increasing distances from the contact points between the pellets.

Finally, Mei *et al* and Tu *et al* attempt to address the problem of the additional capacitance in PBRs introduced by the packing material. Therefere there are three defined capacitances; the dielectric capacitance (C_{diel}), the gas capacitance (C_{gas}), and the packing capacitance ($C_{packing}$). The packing, being composed of many dielectric spheres in the discharge gap, would show a very complex capacative behaviour. In order to simplify the system, the capacitance contributions from the gas and packing are treated as two parallel plate capacitors in series, hence the overall cell capacitance (C_{cell}) is determined by:

$$\frac{1}{C_{cell}} = \frac{1}{C_{diel}} + \frac{1}{C_{gas}} + \frac{1}{C_{packing}}.$$

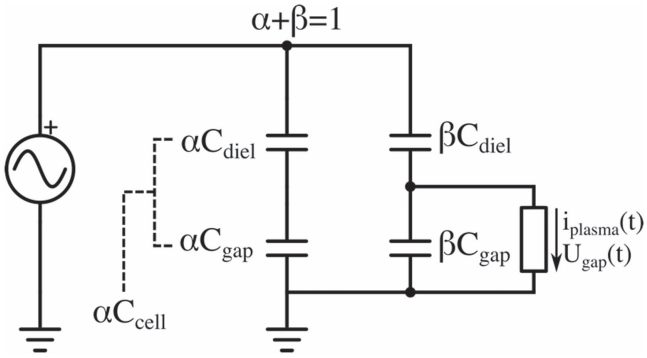

Figure 4. DBD Partial discharging described by Peeters *et al* [25]. The circuit is split into a non-discharging (α) and discharging (β) fraction.

In this model the minimum capacitance that can be measured is based on all capacitance components in series, i.e. C_{cell}. Conversely, it is stated that during the discharging phase the plasma can 'bridge' across the packing and the gas, and the contribution of these terms ($C_{packing}$ and C_{gas}, collectively giving C_{gap}) to the instantaneous capacitance would be negated, leading to the maximum instantaneous capacitance to be C_{diel}. There are some inconsistencies in this 'parallel plate model' that are revealed when the effective capacitance (ζ_{diel}) changes as a function of applied voltage (similar to Kriegseis). Furthermore, Mei *et al* show that dielectric packings, compared with the empty reactor case, increase the value of ζ_{diel} for any given reactor power. This is interpreted as packing materials increasing 'charge bridging'. However, the value of C_{cell} also changes with the presence of the packing material, increasing it for higher dielectric constant materials. Given that the measured value of ζ_{diel} for any given reactor set-up has a possible range between C_{cell} and C_{diel}, there is a possible scenario where ζ_{diel} in one reactor (i.e. with 'some' plasma and no packing) is less than the value of C_{cell} in another reactor (i.e. no plasma and a high dielectric constant packing). Therefore, the value of ζ_{diel} should be normalised against C_{cell} and C_{diel} in order to give a fair comparison when different packing materials are used.

Here it is assumed that normalisation of ζ_{diel} between C_{cell} and C_{diel} yields the identical equation used to calculate α in the Peeters partial discharging model (i.e. equation (2)). However, in this work the value of α is not just dependent on the areal fraction of the electrode discharging, but also the extent of 'charge bridging' across the discharge gap. The alpha values, being the normalised capacitance, can have a value between 0 and 1. A value of zero indicating complete charge bridging in the reactor, and a value of 1 indicating no charge bridging (i.e. no plasma present). There are two possible origins of partial discharging in PBRs; non-discharging of part of an electrode, and plasma discharges not 'bridging the gap' between the electrodes. Full reactor discharging occurs when all of the charge on one electrode is transferred to the opposing electrode during the discharge cycle. In a PBR, each packing pellet acts as an individual capacitor and can therefore trap charges. The point-to-point discharges (described as 'polar' in this work) observed in PBRs, as well as the abundance of partially discharging PBRs in literature are evidence of this [7, 26–28].

One of the important outcomes of the partial discharging circuit of Peeters is that reactor characteristics (e.g. burning voltage and conductively transfer charge) are misestimated when read directly from the QV plots. Indeed, the applied voltage dependent value of ζ_{diel}, combined with the almond shape of the Q–V plot suggests that there is a variable burning voltage in PBRs. This further implies that reduced field calculations and their derivatives for PBRs (as shown in [7, 28]) based on the Q–V diagrams are invalid. Previous studies in situations where there is a variable burning voltage suggest that the instantaneous value of $\mathrm{d}Q/\mathrm{d}V$ can have no physical interpretation [29].

In the majority of publications to date on packed bed reactors, where the reactor capacitances are reported, partial discharging appears to be a very common phenomenon. This has two implications; 1—plasma discharge characteristics are not being correctly reported, and 2—packing materials are not being tested under equivalent operating conditions. The latter point is the most important, given that often these studies are primarily being done to study material catalytic properties and their effect on gas conversion and efficiency. If it is believed that the plasma activates the catalyst, and therefore that good plasma-surface interaction is important, it therefore follows that in order to test catalysts, comparable plasma-catalyst interaction between experiments is desirable for a fair test. In section 3.4 of this work, we show that, even with identical measured conditions, the mechanism of plasma formation and the plasma-surface interactions can be very different between different materials.

Packed bed reactors should have an alternative equivalent electrical circuit that reflect the capacitive properties of the pellets and the resultant tendency of the reactor towards partial discharging. An equivalent circuit model for PBRs should accommodate the two types of 'partial discharging' in PBRs: electrode area non-discharging, and polar discharges (i.e. 'point-to-point' discharges). To accommodate the polar discharge and the variable burning voltage of the PBR there needs to be time dependent capacitance terms that contribute towards calculation of partial discharging.

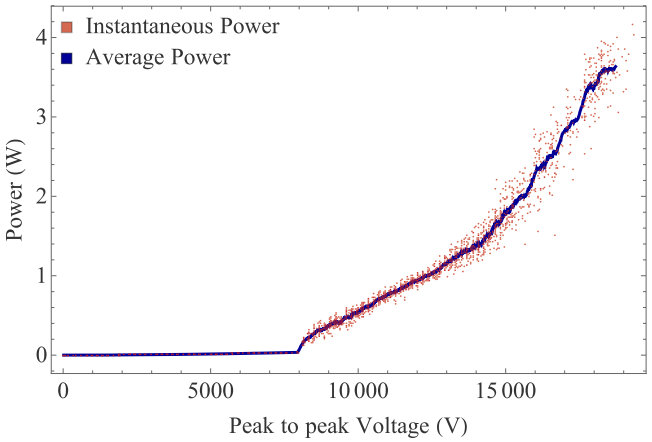

Figure 5. The voltage–power profile of the single pellet reactor discharging in air in DBD mode, i.e.—without a pellet with a sub mm electrode separation. The points representing the instantaneous power shows the power discharged in one individual AC cycle. By applying this method, instabilities in the plasma behaviour can be observed in the experimental data.

This model is not within the scope of this article but should be developed in future.

However, in the absence of the full mathematical formulation corresponding to this equivalent circuit, the same 'partial discharging' circuit of Peeters can be applied, keeping in mind that the interpretation of the parameter α is not the same as it is for a pure DBD. The limitations of this model are reflected in figure 11, as ζ_{diel} can take a range of values for any given applied voltage when the Q–V plot deviates significantly from the classic parallelogram shape.

The remainder of the article explores the electrical characterisation of packed bed reactors through the use of a single pellet DBD reactor. The electrical dynamics of the two different discharge types, bridging streamers and point-to-point discharges, in PBRs are investigated. This is achieved by the application of a unique analytical technique based on the rapid analysis of sequential Q–V plots, as well as Peeters' partial discharging equivalent circuit. Further discussion on the origin of the almond shaped Q–V plots observed with the SPR (and PBRs) is given in section 3.6.

2.6. Features of methodology

In order to assist with interpreting the presented data, the implementation of the methodology is described.

2.6.1. Instantaneous power measurement. It is stated in the LabVIEW method section that consecutive QV plots are analysed. The image in figure 5 shows the results from applying the LabVIEW programme to the reactor operating as a DBD, i.e. with no pellet present. The average power line shows the power measurement that would be expected if many Q–V plots were averaged. Each data point represents the QV plot data from individual AC cycles. It is apparent from this plot that there is actually variation in the power

discharged in the DBD on consecutive cycles. This is a useful technique when applied to the single pellet reactor as some of the discharging modes are inherently unstable, and do not repeat identically on consecutive cycles (this is shown in section 3.2). This instability can be observed by measuring the power difference from one AC cycle to the next, and observing the distribution of discharge powers, rather than one average power. It should be noted that in a classic DBD, plasma power scales linearly with applied voltage. However, the unusual shape of the electrodes used here (i.e. dome shaped live electrode with a small indentation), combined with their small area yields a voltage–power relationship that shows two linear dependencies.

2.6.2. Determination of capacitances and measurement of 'α coefficient'. Alpha is calculated using equation (2). This requires C_{diel} to be known for the reactor, C_{cell} to be calculated for each different pellet used, and for ζ_{diel} to be calculated for each QV plot. C_{diel} is determined solely by the thickness, material and dimensions of the dielectric layer, and is therefore fixed for any given reactor geometry. For clarity, it needs to be restated that the value of C_{diel} is independent of the pellet capacitance. C_{diel} can be calculated using the equation for a parallel plate capacitor, given by equation (3):

$$C_{\text{diel}} = \frac{k\epsilon_0 A}{d}, \tag{3}$$

where k is the relative permittivity of the alumina dielectric (9–11), ε_0 is the permittivity of free space, A is the electrode area (calculated from the diameter, 5.5 mm), and d is the thickness of the dielectric (0.5 ± 0.05 mm). This gives a value for C_{diel} of ∼5 ± 1 pF. The value for C_{cell} is measured in each experiment based on the gradient of the non-discharging lines of the Q–V plot. A decrease in the value of C_{cell} with increasing applied voltage is observed in all experiments, with a change in value of up to 9%. A similar phenomenon is also described in [25], but the origin of this behaviour is not known. In the calculation of α, C_{cell} is measured at each voltage to compensate for this behaviour.

ζ_{diel} is measured by linear regression, applying a weighted least squares fitting method to find the gradient of the discharging lines of the Q–V plot. The shapes of the Q–V plots obtained in these experiments are irregular, and do not conform the ideal parallelogram obtained in a typical DBD experiment. This indicates that the electrical behaviour of the single pellet reactor (or packed bed reactors), does not conform to the idealised behaviour represented by the classical or partial discharging DBD parallelogram. The reason for this non-ideal behaviour is discussed further in sections 3.4–3.6.

To avoid the implications of this problem, and in the absence of a better equivalent circuit model, the partial discharging model can be applied by accounting for the range of possible values for $\zeta_{\text{diel.}}$ In order to do this the gradient of the line ζ_{diel} is measured four times (shown in figure 6): for the positive ($^{+}\zeta_{\text{diel}}$) and negative parts ($^{-}\zeta_{\text{diel}}$) of the discharge cycle, and for a maximum ($\zeta_{\text{diel-max}}$) and minimum ($\zeta_{\text{diel-min}}$) possible value for ζ_{diel} for each of these cycles. To clarify,

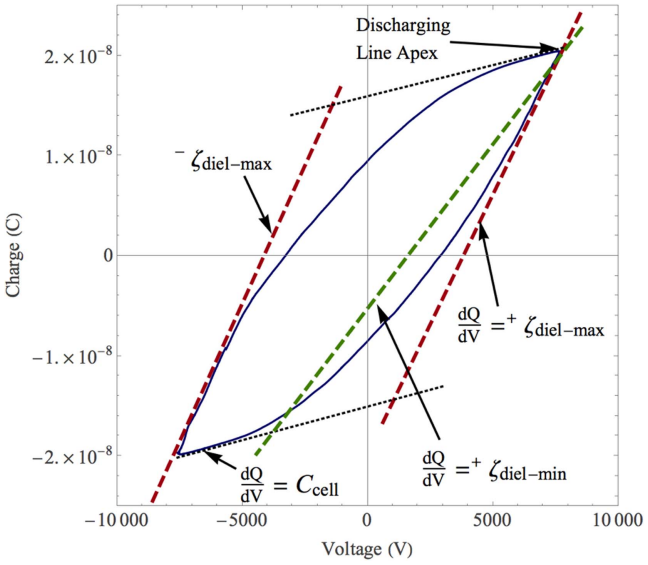

Figure 6. Approximate position of measurement for the effective dielectric capacitance terms (ζ_{diel}) used in this work. The value of ζ_{diel} is measured four times, during the positive ($^{+}\zeta_{\text{diel}}$) and negative ($^{-}\zeta_{\text{diel}}$) half cycles, and for maximum ($\zeta_{\text{diel-max}}$) and minimum ($\zeta_{\text{diel-min}}$) possible values. The value for the $\zeta_{\text{diel-max}}$ discharging line gradient is measured at the steepest point from the apex of the line using a weighted least squares method. $\zeta_{\text{diel-min}}$ is determined, also using the same weighted least squares averaging method, to an arbitrary point corresponding to the approximate start of the discharging period. The weighting is applied by setting the weight of the co-ordinates of the apex such that they become a fixed point. The Q–V plot shown here is for a $BaTiO_3$ pellet, and illustrates how the equivalent circuit model for a DBD (that yields a parallelogram) does not apply to a packed bed DBD.

linear regression is used to find $\mathrm{d}Q/\mathrm{d}V$ at the end of the discharging phase ($\zeta_{\text{diel-max}}$), and at from the beginning to the end of the discharging phase ($\zeta_{\text{diel-min}}$). This effectively allows the application of the classic DBD equivalent circuit model with a non-classical case. Hence, the wider the range of these measured values provides information regarding the deviation from the classic model. Therefore, for a classic parallelogram Q–V plot the difference between $\zeta_{\text{diel-max}}$ and $\zeta_{\text{diel-min}}$ would be zero.

Furthermore, the measurement of $\zeta_{\text{diel-max}}$ is complicated in some cases (namely SiO_2 and Al_2O_3 at high voltages) by the 'steps' that occur in the Q–V plot corresponding to streamers carrying a large charge. The origins of these steps is complex, which may be related to the polarisation rate of the dielectric, and is perhaps worthy of its own discussion in the future. This 'step' problem can be eliminated by two means: 1—averaging many (500 or so) Q–V plots, 2—taking the max gradient of the negative part of the discharge cycle ($^{-}\zeta_{\text{diel-max}}$) where the steps are not observed. In this article, the former method is limited to 40 cycles, and hence the latter method is used.

We assume that each of the values measured for ζ_{diel} are equivalent to the effective dielectric capacitance as described in the partial discharging model of Peeters and van de Sanden [25], despite the Q–V plot not having the classic parallelogram form. The value of α is therefore calculated four times

Reactor Condition	Plasma Off	Polar Townsend	Polar Streamer	Unstable Streamer	Stable Streamer
Example Voltage	4 kV	9 kV	11.5 kV	13.5 kV	17 kV
Alpha value	1	0.997	0.95	0.6	0.1
Image					
Q–V Plot	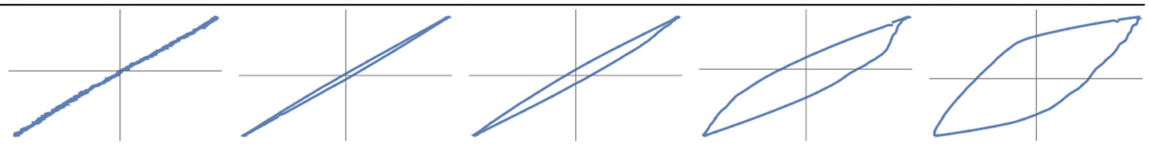				

Figure 7. Relationship between applied voltage and the formation of plasma in the single pellet reactor using a YSZ pellet in N_2. Five different reactor operating conditions are identified, with their corresponding average Q–V plots(based on 40 Q–V plots) and calculated 'alpha values', a variable which quantifies the extent of partial reactor discharging. The images of the plasma are taken from video stills from the corresponding video provided in the supplementary information.

for each value of ζ_{diel}, each time using equation (2), and in the plots where α is used, every calculated value is plotted.

3. Experimental results

3.1. Relation between voltage, plasma ignition and discharge regime

The results section offers a description and electrical characteristics for a number of different plasma discharge regimes. Example videos for each material are provided with the supplementary information, available online. Figure 7 presents video screenshots of the different discharge regimes, together with some representative data for the YSZ pellets. Images of the two primary discharge modes, polar and streamers discharges, together with some further subcategories of discharge type, are shown.

From the video data the threshold voltage for plasma ignition and streamer formation are obtained. Plasma ignition is defined as the voltage at which any plasma forms in the reactor, whereas streamer formation is the threshold voltage for plasma breakdown that propagates between the electrodes.

Figure 8 shows the ignition and streamer onset voltages for each of the different pellet materials tested. With increasing dielectric constant, the threshold voltage for plasma ignition decreases. Conversely, with increasing dielectric constant the threshold voltage for streamer onset increases. However, these two simplistic statements mask the more complex behaviour that is actually occurring.

Plasma ignition with YSZ, $CaTiO_3$ and $BaTiO_3$ occurs, without exception, at the poles of the pellet at the electrode-pellet interface. Whereas plasma ignition with Al_2O_3 always transitions directly into the streamer discharge regime without any prior 'polar' discharge. The behaviour with silica at plasma ignition is less predictable, with three different discharge behaviours observed: 1—polar ignition followed by stable streamers; 2—stable streamer ignition; 3—streamer ignition followed by transition to the polar regime.

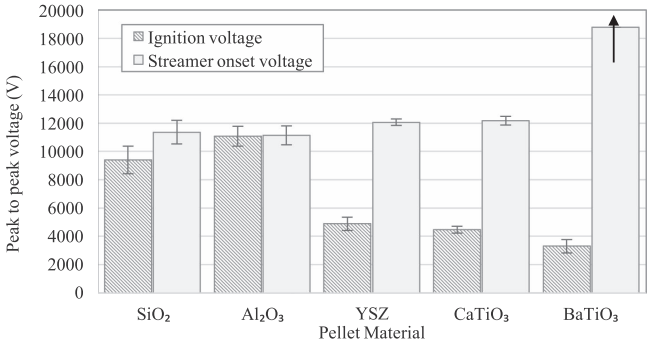

Figure 8. Threshold voltages for the two major discharge regimes observed. Dielectric constant for the materials tested increases from left to right. The arrow at the top of the $BaTiO_3$ graph indicates that the threshold voltage for bridging streamers could not be reached with the experimental set-up used.

The transition from the polar to the streamer regime marks a significant change in plasma behaviour. Besides this, the behaviour of the plasma with each packing material also shows a range of behaviours. Based on these behaviours it is possible to group the materials into 'low' (SiO_2 and Al_2O_3), 'medium' (YSZ and $CaTiO_3$), and 'high' ($BaTiO_3$) dielectric constant materials.

Firstly, we will discuss the medium dielectric constant materials, YSZ and $CaTiO_3$, as they both exhibit very similar behaviours. The plasma discharge ignites in the polar regime, and expands radially outwards with increasing voltage. With the YSZ, the polar discharge ignites as a homogeneous glow at the dielectric-YSZ interface, this appears to be an atmospheric pressure glow discharge (APGD) [30]. With increasing applied voltage this transitions to a polar confined streamer discharge. This transition is characterised by instability, and is seemingly related to the onset of streamer formation at the uncoated live electrode. With the $CaTiO_3$, plasma ignites directly in this polar confined streamer mode,

although this may be due to the relatively uneven, and rough surface of $CaTiO_3$ compared with YSZ. Once the streamer transition threshold voltage is reached, streamers begin to propagate from the uncoated live electrode towards the dielectric coated ground across the pellet surface. As the applied voltage is further increased, the number and density of these streamers increases. The streamers appear to be bound to the surface of the pellet, exhibiting a very strong interaction in both cases.

The low dielectric constant materials have the highest plasma onset voltage, but the lowest transition voltages to the streamer regime, and upon streamer formation there is a weaker plasma-packing interaction. At the ignition voltage with the low dielectric constant materials, there is a similar plasma-surface interaction that is seen with the medium dielectric constant materials i.e. streamers propagate close to the surface of the material. However, as voltage is further increased, in some cases formation of a DBD like streamer occurs. That is, the streamer does not tend to propagate over the pellet surface, but away from the material surface in the gas phase. It should be noted that when the reactor is operated in DBD mode (i.e. no pellet) with a similar gap spacing to those when a pellet is present, it is not possible to form a plasma.

Finally, with the high dielectric constant material the transition from the polar regime to the streamer regime does not occur within the voltage range of the amplifier (i.e. less than 19 kV peak to peak, at 10 kHz.) Instead, the polar discharge expands radially outwards across the pellet with increasing voltage. The plasma appears to feature a large number of highly intense, localised streamer discharges that form between the poles of the pellet and the electrodes. The inter-electrode gap never appears to be bridged by the streamers.

3.2. Voltage–power plots and their relationship to plasma behaviour

A comparison of the transition voltages shown in figure 8 and the voltage–power plots for each packing material reveals how the observations of plasma behaviour relate to measurements made using the measurement circuit.

In the video experiments, two significant voltage transition points in behaviour are defined: the plasma ignition and the polar to streamer transition.

Figure 9 shows a comparison of the observed transitions occurring from the video, marked by vertical lines, with the measured voltage–power data from the experiment using YSZ. The points indicate the average reactor power consumption in each period of the applied sine wave. This data is obtained, as stated in the methods section, from 'single shot' *Q–V* plots. The solid line represents the moving average of this power. Each different identified regime from the video data has its own voltage–power profile. Using the YSZ pellet as an example, the voltage–power behaviour of each region of the graph is explained:

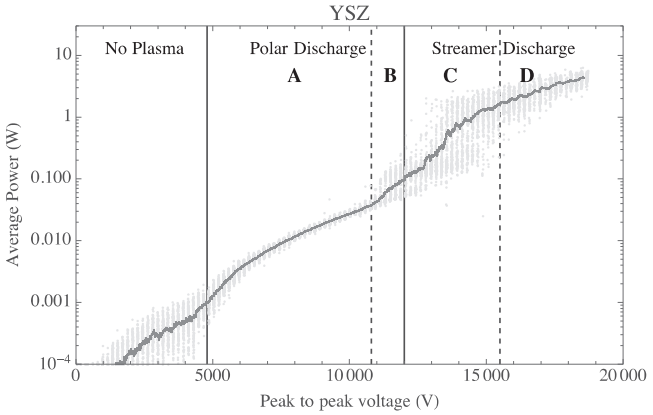

Figure 9. YSZ voltage–log power plot. The labelled regions correspond with the plasma behaviours described in figure 7. That is: A—polar Townsend, B—polar streamer, C—unstable streamer, D—stable streamer. The light grey points represent the power based on individual *Q–V* plots corresponding to a single AC discharge cycle of the reactor. The dark grey line represents the moving average of three repeats of the experimental data. Note that the regions with broad distributions in the light grey points effectively reflect unstable behaviour, where plasma behaviour is different on consecutive AC cycles.

1. *No Plasma region*—There is a small power consumption ($<10^{-3}$ W) that increases with increasing voltage. This power consumption may be due to dielectric losses (i.e. Tan δ losses) in the pellet and dielectric layer. However, power measurement on this scale via the *Q–V* plot method is particularly susceptible to electronic interference from the high voltage power source. Stray inductance and capacitance can lead to significant interference in the oscilloscope probe. Hence, no conclusions should be made regarding dielectric losses in this region of operation.
2. *Polar Discharge Region*—At higher applied voltages, the plasma 'ignites' and the polar discharge regime begins (region A in figure 9). Power consumed in the reactor steadily increases, from 0.001 W at ignition (4900 V peak to peak) up to 0.05 W at ~10000 V. The consistent and stable low power consumption in the region from 5000 to 10000 V reflects the observation from the video data that the plasma formed is an APGD. At the 10000 V point, a transition in the plasma behaviour in the video is observed, with the voltage–power data reflecting this transition (region B in figure 9). This appears as an increase in the power discharged on some cycles, and a wider range of measured powers on consecutive discharge cycles. The characteristics of the discharge change to that of a streamer discharge localized at the poles of the pellet. We can therefore split the polar discharge region into two further discharge types—a polar Townsend discharge region occurring at lower voltages, and a polar streamer region at higher voltages.
3. *Streamer discharge region*—At voltages greater than 12000 V streamers begin to propagate across the pellet (region C in figure 9). This transition is accompanied by

a large step increase in plasma power from 0.1 to 0.2 W (low power) up to 0.5–4 W (high power) or higher. Figure 9 shows that in the region from 12000 to 15000 V, that some of the discharging cycles are low power, and some are high power, i.e. this is a transition region with an unstable plasma discharge. In this transition region, the plasma discharge type alternates between bridging streamer and polar discharges on consecutive cycles. As the applied voltage to the reactor is increased, the number of consecutive AC cycles in which streamer discharges occur also increases. At voltages in excess of 15000 V, only the high power discharge occurs and therefore streamers propagate across the pellet on every discharge cycle (region D in figure 9). We can therefore define a further two discharge types in the streamer discharge regime, an unstable streamer transition region and a stabilised streamer region.

The relationship between the plasma behaviour and the form of the voltage–power plots for other materials is explained further into section 3.4, alongside the coefficient α, which is used to quantify partial discharging.

3.3. Relationship between plasma behaviour and alpha coefficient for YSZ

In our previous work, we applied an alternative equivalent circuit developed by Peeters *et al* to packed bed reactors where we quantified and demonstrated the impact of partial discharging [21]. In this article, with the SPR, it is possible to add a plot of the partial discharging coefficient, alpha, to the voltage–power profile of each material. The value of alpha is calculated from the value of ζ_{diel}, the effective dielectric capacitance, as described in section 2.5. The Peeters model is based on partial discharging in a classic DBD. However, for PBRs the equivalent circuit model deviates from the classical DBD behaviour, in that there is a voltage dependence to the value of ζ_{diel}.

Figure 10 shows the measured capacitance values for all of the possible capacitances that can be measured for the *Q–V* plots for YSZ. There are two sets of two values for ζ_{diel}, corresponding to the positive and negative parts of the discharge cycle, and the possible maximum and minimum values. This distribution of values is a direct result of trying to apply the partial discharging model, an extension of the classic DBD behaviour, to a non-classical scenario. The lower capacitance values are represented by the green points, indicating the measured values for C_{cell} during the positive ($+C_{\text{cell}}$) and negative discharge ($-C_{\text{cell}}$) cycles. The measured values show a very narrow distribution and are highly repeatable on consecutive cycles, showing that this measurement is very stable. However, there is a 9% decrease in the value of C_{cell} at high input voltages that has an unknown origin, and is also described in [25].

The measured values for ζ_{diel} show a much broader distribution, particularly at input voltages in excess of 12 kV peak to peak. The low values for ζ_{diel} ($\zeta_{\text{diel-min}}$) take a least squares

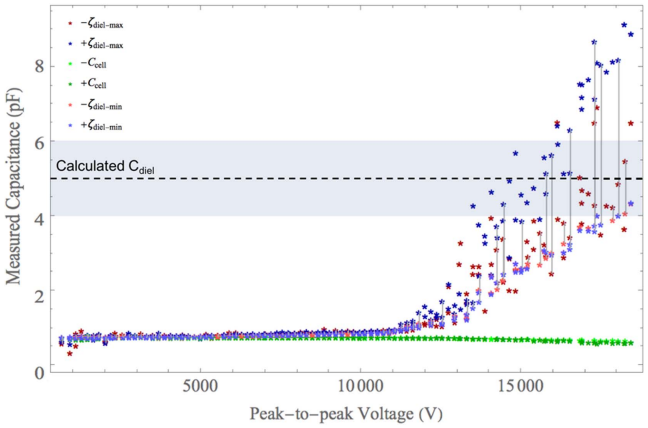

Figure 10. Capacitance measurements for YSZ as a function of voltage. C_{cell} for the positive and negative half cycles are measured (green points). ζ_{diel} is measured and maximum (dark points) and minimum (light points) values for both the positive (blue) and negative (red) AC cycles are determined. Maximum and minimum points measure in the same half cycle are connected by grey lines. The calculated value of dielectric capacitance ($C_{\text{diel}} = 5 \pm 1$ pF) is plotted as a pale blue band.

fit from the apex of the *Q–V* plot, to the point at which the measured value for capacitance begin to deviate from the measured value for C_{cell} (as shown in figure 6). The high values of ζ_{diel} ($\zeta_{\text{diel-max}}$) are measured, using a least squares fit, at an arbitrary point close to the apex of the *Q–V* plot. The high and low measurement points, $\zeta_{\text{diel-max}}$ and $\zeta_{\text{diel-min}}$, therefore represent the range of values of ζ_{diel}. $\zeta_{\text{diel-max}}$ and $\zeta_{\text{diel-min}}$ obtained from the same *Q–V* plot are connected by grey lines to indicate the range of values ζ_{diel} could have. Additionally, it should be noted that the calculated dielectric capacitance, C_{diel}, has a value of 5 ± 1 pF, this is plotted as a horizontal band in figure 10. In some cases, namely with $\zeta_{\text{diel-max}}$, the measured value exceeds the calculated value for C_{diel}, theoretically this should not be possible. This is caused by the previously described 'steps' in the *Q–V* plot, for further discussion of this see section 2.6.2. At high voltages, the measured value for $\zeta_{\text{diel-max}}$ on the positive half cycle is frequently higher than during the negative half cycle, again, this is caused by 'steps' that occur more frequently in the positive cycle (these steps are also described in [31]). The measured values of ζ_{diel} can be used to calculate α, and hence quantify partial discharging in the reactor. As stated previously the value of α can be between 0 and 1. When the value of ζ_{diel} exceeds C_{diel}, α becomes negative. This does not reflect a physical phenomenon, but rather a limitation in current methods to measure the dielectric capacitance in non-classical DBDs where 'steps' are present in the *Q–V* plot.

Figure 11 shows how the alpha coefficient varies with applied voltage and plasma power for the different tested materials. In the original equivalent circuit devised by Peeters et al for DBDs [25], a low value of alpha is indicative of a greater areal fraction of the electrode discharging. However, the original equivalent circuit is explicitly devised for DBDs. The SPR shown here, and indeed PBRs in general, have an equivalent circuit that must take into account the capacitance of the packing material and the possibility of partial

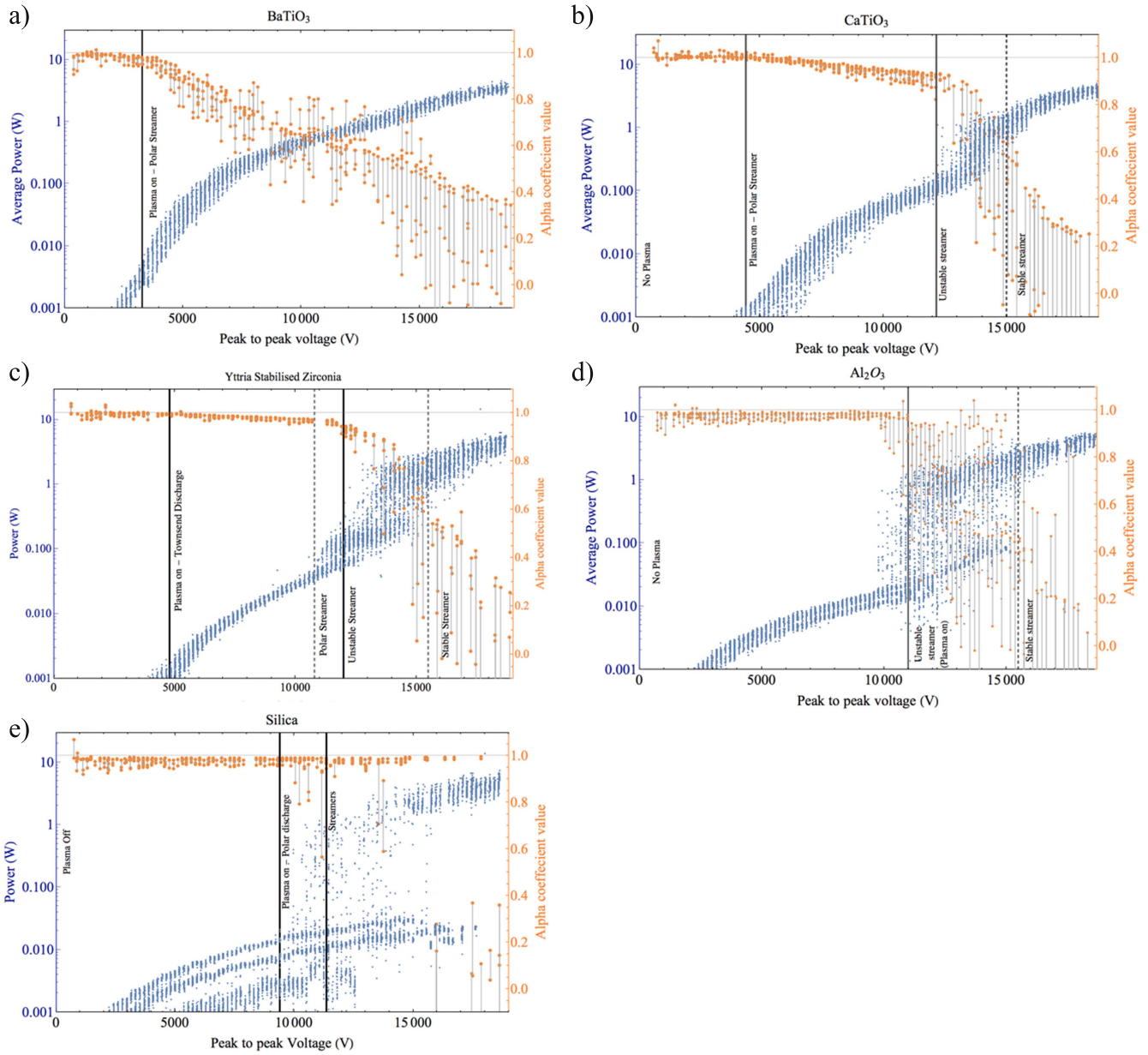

Figure 11. Voltage–log power and alpha plots for: (A) YSZ, (B) $CaTiO_3$, (C) $BaTiO_3$, (D) Al_2O_3, (E) silica. Each plot is the accumulation of data from three experimental repeats. Similarly to the the effective capacitance measurement, the grey connecting lines join the maximum and minimum α values measured per discharge cycle.

discharging. The alpha coefficient in this instance can be considered as the fraction of charge conductively transferred between the electrodes i.e. if the alpha coefficient has a value greater than 0, the packing material is acting capacatively during the discharge phase. The higher this value, the greater the contribution of the packing capacitance to limiting charge transfer between the electrodes in the discharging phase of the reactor. This is significant as it reflects to what extent plasma 'bridges the gap' between the electrodes, and therefore could be used as a measure of plasma—catalyst contacting.

In figure 11, it can be seen that when the plasma is off, the alpha coefficient value is $\sim$1. With increasing voltages, the alpha value generally tends to decrease, approaching 0 at the highest applied voltages. In the polar discharge regimes (Townsend and polar streamer regions) there is a small, but noticeable decrease in the alpha value. As the plasma discharge progresses into the streamer regime, due to the increase in applied voltage, the alpha value decreases more rapidly. This rapid decrease in alpha is due to charge being transferred across the gap, rather than being 'trapped' by the pellet. Higher dielectric constant materials are likely to have a higher capacity to trap charges, so it is expected that there will be a relationship between applied voltage, alpha, and material dielectric constant.

Figures 11(A)–(E) show the voltage–power relationships and alpha coefficients for the other dielectric materials tested.

Through addressing the medium dielectric constant materials first, the influence of the pellet capacitance on the charge transfer in the reactor may be elucidated. Comparing the two medium dielectric constant materials, YSZ (figure 12(C)) and

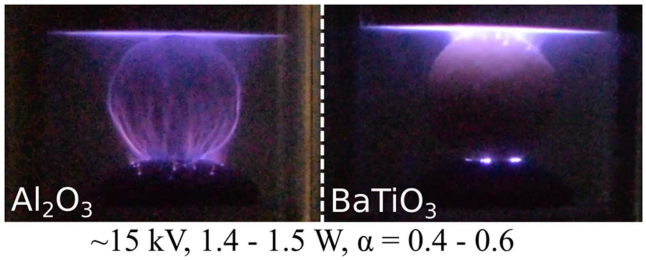

Figure 12. Example screenshots of the plasma from the Al_2O_3 and $BaTiO_3$ examples, where the voltage, power and alpha coefficient are equivalent. This example illustrates that although plasma properties can, to some extent, be quantified using the techniques demonstrated in this article, that the real behaviour of the plasma is not reflected in the numbers.

$CaTiO_3$ (figure 12(B)) in the polar discharge region we can make three statements:

(1) Plasma behaviour in this regime is relatively stable, having similar discharge powers and alpha coefficients on consecutive cycles.
(2) Plasma generation is localised at the poles, this is confirmed by the video data and the low value of α.
(3) Higher dielectric constant materials have a higher capacity to trap charges. With the higher dielectric constant material, $CaTiO_3$, the voltage—α gradient (figure 11(B)) is steeper than with the YSZ in the polar discharge regime. Additionally, the plasma power at any given applied voltage is higher with $CaTiO_3$ than with YSZ. The voltage–power profile for $CaTiO_3$ shows that a larger plasma current is generated, and that the pellet has a higher capacity to 'trap' the generated charges. This 'trapping charges' theory can also be confirmed by observing that the transition into the streamer regime happens at a higher plasma power, and higher value for α with $CaTiO_3$ than with YSZ.

Looking at the voltage–power and alpha plots for $BaTiO_3$ and Al_2O_3 helps to give further weight to these ideas, i.e. that high dielectric constant materials trap charges. For example, it can be seen from the $BaTiO_3$ plot (figure 11(A)), and corresponding video data that the transition to the streamer regime does not occur. Despite this the alpha coefficient value decreases to the range ~0–0.4 at the maximum applied voltage. This indicates that the majority of the charges that are generated in the plasma are trapped by the packing material at the poles of the pellet i.e. the plasma does not propagate between the electrodes, but between the poles of the pellets and the electrodes. Within the polar discharge region for $BaTiO_3$, the gradient of the voltage-alpha line is steeper than with the other materials. This supports the point described previously, that plasma generation is localized to the poles of the pellets, and that high dielectric constant materials trap charges.

The voltage–power relationship and alpha plot for the Al_2O_3 pellet (figure 11(D)) show a more complex behaviour. During the no plasma regime, the alpha coefficient remains at 1. Once the unstable streamer regime is reached, the voltage–power profile and video data indicate that the reactor transitions immediately into a surface streamer mode that bridges charge between the pellets. The surface streamers occur irregularly, with plasma formation not always occurring on consecutive discharge cycles. As the applied voltage is increased, the probability of streamer discharges bridging the gaps in an AC cycle is increased. As the voltage is increased through the unstable streamer regime, the measured alpha coefficient value decreases. The measured alpha coefficient is based on the average *Q–V* plot from 40 consecutive AC cycles, therefore the average alpha coefficient must also indicate the probability of charge transfer between the electrodes in the reactor. In the stable streamer regime, the majority of the measured alpha values are less than 0.2. This indicates that almost all stored charge is transferred between the electrodes on every discharge cycle, with the pellet itself trapping few charges.

Finally, the voltage-profile for the plasma with SiO_2 (figure 11(E)) can be addressed. As described previously, and as shown by the video data, the behaviour of the plasma with a SiO_2 packing is erratic. Despite the data shown in figure 11(E) being based on 3 repeats, with more experimental repeats being attempted, it was not possible to obtain stable, repeatable data with this material. This is the lowest dielectric constant material out of all of the tested materials, so it could be possible that due to a lack of localized electric field enhancement, other material properties that influence plasma formation may be having a dominant effect. This may mean that surface defects, moisture or sample contamination may influence the experimental outcomes. It is worth noting that the alpha coefficient value in figure 11(E) at some particularly high voltages extends to a value far below zero (−1 in some cases). This is attributed to a 'flashover' effect, this is where violent, spark like discharges propagate between the electrodes, transferring a large charge that extends beyond the front face of the ground electrode.

3.4. Q–V plots and plasma behaviour

The use of the voltage–power plots and alpha coefficients are useful in trying to quantify some of the plasma behaviours observed in the videos. However, there are scenarios where identical values could be obtained for voltage, power and alpha coefficient, despite their being significant differences in plasma behaviour, as shown in figure 12. A qualitative assessment of the corresponding *Q–V* plots (figure 13) reflects these differences in the type of the plasma discharge, i.e. polar discharge or bridging streamers. The *Q–V* plot for alumina approximates the characteristic parallelogram of a DBD. The rounded edges, and 'wobbly' discharging lines of the alumina *Q–V* plot originating from asymmetry in the discharges, and stepped edges due to the presence of individual streamers [31], being averaged from 40 consecutive AC cycles. The *Q–V* plot for barium titanate is 'almond shaped', featuring curved transitions from the capacitive to the discharging regions of the *Q–V* loop. This shape has been observed previously with packed bed DBD with a $BaTiO_3$ packing [21], as well as plasma actuators [32]. Note that this shape is not exclusive to barium titanate in the SPR, but is also observed

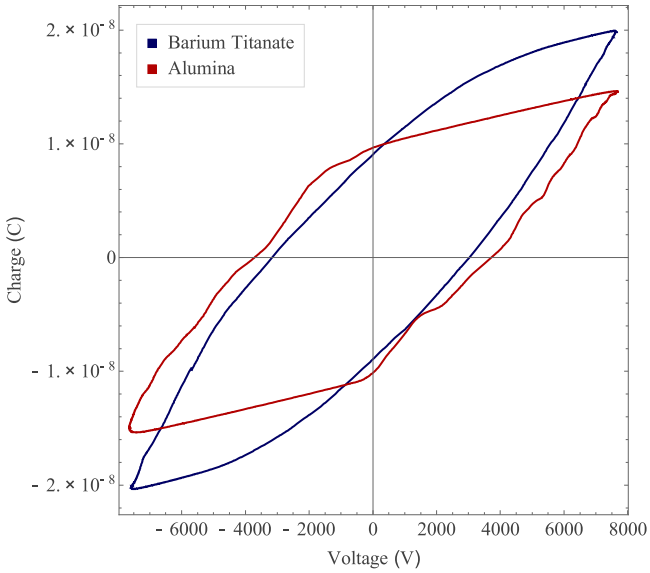

Figure 13. *Q–V* plots approximately corresponding to the images shown in figure 12. The *QV* plots are based on the averages of 40 consecutive AC cycles. The area of the plots, the voltages, and the gradients of the discharging lines are similar (from which alpha is calculated). The two major differences between the *Q–V* plots are the maximum amplitude of the charge, and the shape.

with YSZ and $CaTiO_3$ when operating in the polar discharge regime. This 'almond shaped' *QV* plot is very repeatable over consecutive AC cycles (this is reflected in the voltage–power profiles), and is characteristic of the polar discharge regime. Given the limitations of the values of the voltage, power, and alpha coefficient in describing the behaviour of the plasma, for future researchers a qualitative assessment of the *Q–V* plot could provide a useful insight into the behaviour of the plasma. The reasons that polar discharges lead to an almond shaped *Q–V* plot is explained in section 3.6.

3.5. Implications for packed bed reactors

This article confirms the reports from previous studies that high dielectric constant materials reduce the applied voltage required for plasma formation due to localised electric field enhancement [19]. This work also demonstrates that this breakdown initially appears as a 'polar discharge', also commonly referred to as a point-to-point or partial discharges, at the contact points between the packing pellets. As the applied voltage increases, the discharge will transition to a streamer discharge. With increasing dielectric constant materials, the transition voltage to the streamer regime also increases, although this transition voltage is likely to additionally depend on other material characteristics, such as surface conductivity and roughness. We have demonstrated that packing pellets can trap charges, limiting the extent of plasma formation in the reactor, and that higher dielectric constant materials have a greater capacity to do this.

These observations are significant, particularly for plasma catalytic reactors. Activation of catalyst surfaces may require direct contact with a plasma discharge. If this is the case, high dielectric constant materials may be limiting catalyst activation by constraining the discharge to the contact points of the pellets. Clearly, this has potential implications for the efficacy of plasma-catalytic treatment of a gas. The alpha coefficient value could be used as an indicator of the extent of plasma formation in these reactors, however it is not yet clear exactly what the interpretation of these values might be. It is apparent that achieving as low a value as possible for the alpha coefficient is good, i.e. indicative of effective charge transfer between the electrodes and extensive plasma formation. However, it is not clear what the target for this value should be and what the implications of having a moderate alpha value are (e.g. alpha = 0.5), especially when operating real packed bed DBDs.

This work also shows that current equivalent circuit models for PBRs are not satisfactory, and that a more comprehensive model should be developed that can more accurately reflect the behaviour of the plasma in the reactors. This could then be used to obtain more useful information about the operating condition of the PBRs.

The future equivalent circuit model should account for the partial discharging behaviour that is typically observed in DBDs, where the alpha coefficient indicates the areal fraction of the electrode that is not discharging [25]. It should also account for the capacitance of the packing materials, and consequently the possibility of plasma forming only at the contact points between pellets.

3.6. Interpretation of almond shaped Q–V plots

One of the interesting observations from this work is that 'almond shaped' *Q–V* plots are observed when operating in the polar discharging regime with the SPR (figure 13). The same phenomenon is also observed in PBRs packed with high dielectric constant materials [21], and with surface discharge plasmas such as plasma actuators [33]. This behaviour can be accounted for by considering the physical interpretation of the *Q–V* plot shape and its relationship to the behaviour of the plasma in the reactor.

Consider that the gradient of the line of the *Q–V* plot at any point indicates the instantaneous capacitance of the reactor. In the SPR, the capacitance of the reactor is composed of the capacitance of the gap, the packing and the dielectric layer (as presented in [7]). During the streamer discharge regime, in an ideal scenario where all stored dielectric charge is transferred between the electrodes, the gap and packing capacitance terms are negated. Therefore, measuring the line gradient of the *Q–V* plot in this case yields the dielectric capacitance. Alternately, if the reactor is operating in the polar discharge regime, both the packing pellet and the gap are acting as capacitors. There is some conductive charge transfer through the gap, and some conductive charge transfer across some of the distance across the pellet. Therefore, their combined capacitance is greater than in the 'plasma off' phase, but less than in the ideal stable streamer discharge regime

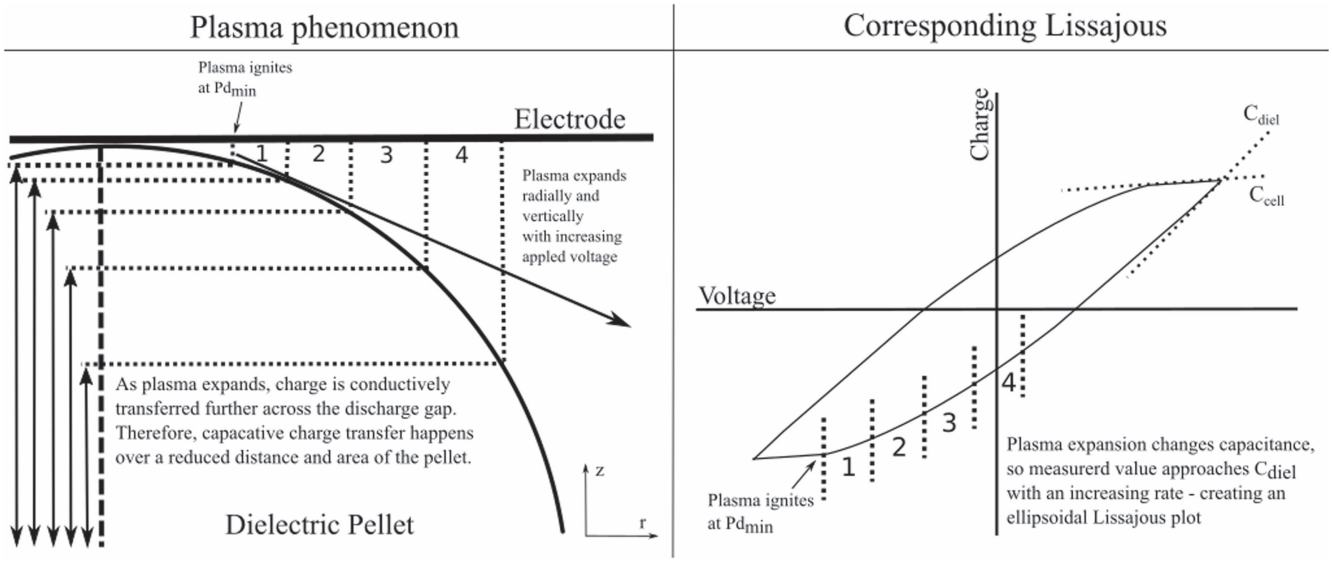

Figure 14. A schematic depiction showing how the polar discharge regime causes the 'almond' shaped *QV* plot to occur.

described previously[3]. In this case the instantaneous gradient of the *Q*–*V* plot would therefore show that the reactor is partially discharging.

With this in mind the plasma behaviour can be related to the 'almond shaped' *Q*–*V* plot (figure 14). It is known that dielectric packing pellets magnify local electric field strengths at the contact points between the pellet and the walls. Indeed, this behaviour is experimentally demonstrated in this work. The maximum field strength occurs at this contact point, particularly with the higher dielectric constant materials. During an AC driven discharge cycle, the gap voltage rises with the external driving voltage. At some threshold voltage the plasma will ignite at a point close to the contact point of the pellet and the dielectric layer, the location of this point will correspond approximately with the Paschen minimum, pd_{min}. As the applied voltage increases, the plasma expands radially outwards from the ignition point to regions where the gap size is larger, and the electric field magnification effect is weaker. Note that there are two compounding effects that influence this radial expansion of the plasma:

1. The electric field is strongest at the contact point and decreases with radial distance form this point.
2. The gap size increases, which as inferred by Paschen's law, requires a stronger electric field to induce electrical breakdown.

As the plasma expands, charge is conductively transferred a greater distance across the gap and the pellet. The further this distance is, the lower the contribution of the gap capacitance and the pellet capacitance to the instantaneous capacitance of the reactor. Therefore, radial expansion of the plasma is observed on the *Q*–*V* plot as the measured value of the instantaneous capacitance approaching the value for the dielectric capacitance.

Consequently, we can state that the Almond shaped *Q*–*V* plots observed with the SPR in polar discharge mode are caused by the plasma igniting at the contact points of the pellets, and expanding radially outwards across the pellet as the applied voltage increases during the AC cycle. The polar discharge theory of the Almond shaped *Q*–*V* plots should also apply to PBRs where multiple pellets are used, regardless of their shape.

An additional and important implication of this observation is that the PBRs do not have one constant 'burning voltage', as DBDs do, but rather a variable one that changes with the expansion of the plasma. This means that using the burning voltage to estimate average electric field strengths (as used in [7, 28, 34]) and therefore electron energies in the reactor is not a valid approximation.

3.7. Unknown unknowns—Plasma induced degradation of YSZ

An additional observation that falls beyond the scope of this paper, but is worthy of inclusion in this article is the plasma induced degradation of the YSZ pellet, shown in figure 15. This demonstrates the application of the SPR for finding the 'unknown unknowns' of plasma-catalysis [35]. It was noted whilst developing the experimental method, that over time the behaviour of the plasma with the YSZ pellet transitioned from a stable streamer discharge to a polar discharge if left at one constant voltage for an extended period of time. This behaviour is observed with N_2, CO_2 and air, but not with noble gasses. This may be due to the higher temperature of the discharge in non-noble gases. The transition in behaviour is also accompanied by the apparent degradation of the YSZ, characterised by the formation of a black ring at the location of the polar discharge. Additionally, the *QV* plot corresponding to the transitions shifts from a parallelogram with stepped edges, to an 'almond' shaped plot characteristic of a polar discharge. This

[3] The capacitance term corresponding to the pellet and gap capacitances increases as the plasma extends across the pellet, and approaches infinity as it gets closer to the opposing electrodes. This appears counterintuitive, but an infinite capacitance can be considered the same as a short circuit.

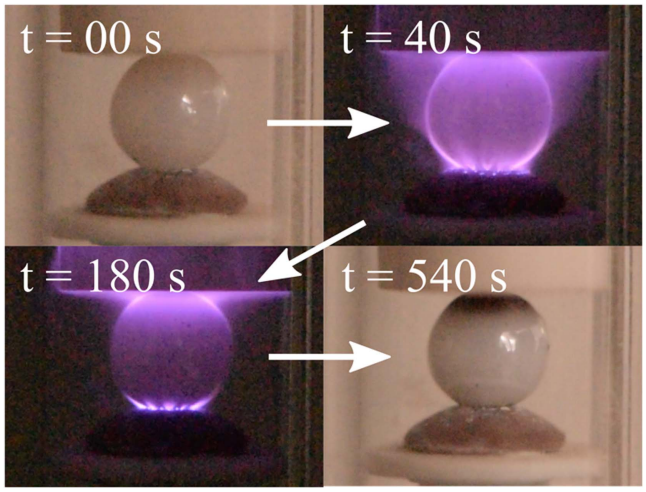

Figure 15. Plasma induced degradation of YSZ with associated change in plasma behaviour observed in an air plasma, discharge transitions from stable streamers to a polar discharge. This degradation is characterised by the formation of a black ring.

'blackening' is reportedly due to electrochemical reduction of the ZrO_2 [36]. If the plasma is switched off, and the pellet allowed to cool, upon reignition of the plasma the discharge ignites in the polar mode. This suggests that this is due to a physical change in the material, rather than a temperature induced change in plasma behaviour.

4. Conclusion

A novel single catalyst pellet DBD reactor (SPR) is demonstrated in this work. The SPR is used to study the influence of material dielectric constant on the dynamics of plasma discharges through electrical characterisation and video of the discharges. This electrical characterisation uses rapid analysis of *Q–V* (aka Lissajous) plots. Voltage–power profiles are obtained for each material, and a phenomenon called 'partial discharging' is quantified.

It is shown that the two main types of discharge observed in PBRs, point-to-point ('polar') and surface streamers have different threshold voltages with different dielectric constant materials. Similarly to previous studies, high dielectric constant materials are found to reduce the voltage of plasma ignition. In moderate and high dielectric constant materials, the plasma tends to ignite first as a polar discharge, whereas with low dielectric constant materials ignition occurs directly in the surface streamer mode. With increasing applied voltage, the plasma transitions from the polar mode to the surface streamer mode. Higher dielectric constant materials increase the voltage of this transition, although this is also likely to also be related to other properties of the material, such as conductivity and porosity.

The polar discharge mode is characterised by the absence of conductive charge transfer between the DBD electrodes. Hence, in this regime plasma formation is observed solely between the electrodes and the poles of the pellet. It is found that the pellet itself is acting as a capacitor, and it 'traps' charges generated in the plasma. This is experimentally verified by applying a recently developed [25] 'partial discharging' equivalent circuit model, which is used to demonstrate that incomplete charge transfer is occurring. Partial discharging may have important implications for catalyst packed DBD reactors, as it reflects the extent of plasma formation in the reactor. Partial discharging is quantified by a coefficient, α, which is based on measurement of the capacitive behaviour of the reactor. The value of alpha ranges between 0 and 1, with 0 indicating complete conductive charge transfer, and 1 indicating no charge transfer and no plasma. In a typical DBD, α represents the areal fraction of the electrodes that are not discharging. In the SPR, α also represents the fraction of charge 'trapped' by the dielectric pellet. Crucially, it is not currently possible in the SPR to differentiate between these two types of partial discharging. This is due to a limitation in applying the classic (or partial discharging) equivalent circuit model of a DDB to a PBR. The recommendation from this work is to quantify partial discharging in PBR experiments, as it can be used to give an indicator of reactor performance. This work has also demonstrated that 'almond' shaped *Q–V* plots occur in the SPR and PBR when the reactor is operating in the polar discharge regime. This provides a qualitative method to understand the behaviour of plasma in a packed bed reactor. Both of these techniques applied together can give a useful insight into the behaviour of plasmas in PBRs.

Acknowledgments

The authors gratefully acknowledge funding for this work from The University of Sheffield and EPSRC under the 4CU Programme Grant (EP/K001329/1). This work was submitted at The University of Sheffield, and further revisions were completed at DIFFER. The author would again like to acknowledge Floran Peeters for useful discussions on this subject.

References

[1] Neyts E C and Bogaerts A 2014 Understanding plasma catalysis through modelling and simulation—a review *J. Phys. D: Appl. Phys.* **47** 224010
[2] Kim H H and Ogata A 2011 Nonthermal plasma activates catalyst: from current understanding and future prospects *Eur. Phys. J. Appl. Phys.* **55** 13806
[3] Kim H-H, Kim J-H and Ogata A 2009 Microscopic observation of discharge plasma on the surface of zeolites supported metal nanoparticles *J. Phys. D: Appl. Phys.* **42** 135210
[4] Kim H-H, Teramoto Y, Negishi N and Ogata A 2015 A multidisciplinary approach to understand the interactions of nonthermal plasma and catalyst: a review *Catalysis Today* **256** 13–22
[5] Kim H-H, Teramoto Y, Sano T, Negishi N and Ogata A 2015 Effects of Si/Al ratio on the interaction of nonthermal plasma and Ag/HY catalysts *Appl. Catalysis* B **166–167** 9–17
[6] Tu X, Verheyde B, Corthals S, Paulussen S and Sels B F 2011 Effect of packing solid material on characteristics of helium dielectric barrier discharge at atmospheric pressure *Phys. Plasmas* **18** 080702

[7] Mei D, Zhu X, He Y-L, Yan J D and Tu X 2015 Plasma-assisted conversion of CO_2 in a dielectric barrier discharge reactor: understanding the effect of packing materials *Plasma Sources Sci. Technol.* **24** 015011
[8] Brandenburg R, Wagner H E, Morozov A M and Kozlov K V 2005 Axial and radial development of microdischarges of barrier discharges in N_2/O_2 mixtures at atmospheric pressure *J. Phys. D: Appl. Phys.* **38** 1649–57
[9] Höft H, Kettlitz M, Hoder T, Weltmann K D and Brandenburg R 2013 The influence of O_2 content on the spatio-temporal development of pulsed driven dielectric barrier discharges in O_2/N_2 gas mixtures *J. Phys. D: Appl. Phys.* **46** 095202
[10] Sewraj N, Carman R J, Merbahi N, Marchal F and Leyssenne E 2011 Spatiotemporal distribution of a monofilamentary dielectric barrier discharge in pure nitrogen *IEEE Trans. Plasma Sci.* **39** 2128–9
[11] Eliasson B, Hirth M and Kogelschatz U 1987 Ozone synthesis from oxygen in dielectric barrier discharges *J. Phys. D: Appl. Phys.* **20** 1421
[12] Akishev Y S *et al* 2011 Role of the volume and surface breakdown in a formation of microdischarges in a steady-state DBD *Eur. Phys. J.* D **61** 421–9
[13] Jidenko N, Petit M and Borra J P 2006 Electrical characterization of microdischarges produced by dielectric barrier discharge in dry air at atmospheric pressure *J. Phys. D: Appl. Phys.* **39** 281–93
[14] Braun D, Kuchler U and Pietsch G 1991 Microdischarges in air-fed ozonizers *J. Phys. D: Appl. Phys.* **24** 564
[15] Drimal J, Kozlov K V, Gibalov V I and Samoylovich V G 1988 On value of transferred charge in silent discharge under atmospheric pressure *Czech. J. Phys.* B **38** 159–65
[16] Aerts R, Martens T and Bogaerts A 2012 Influence of vibrational states on CO_2 splitting by dielectric barrier discharges *J. Phys. Chem.* C **116** 23257–73
[17] Ponduri S, Becker M M, Welzel S, van de Sanden M C M, Loffhagen D and Engeln R 2016 Fluid modelling of CO_2 dissociation in a dielectric barrier discharge *J. Appl. Phys.* **119** 093301
[18] Van Laer K and Bogaerts A 2016 Fluid modelling of a packed bed dielectric barrier discharge plasma reactor *Plasma Sources Sci. Technol.* **25** 015002
[19] Van Laer K and Bogaerts A 2016 Influence of gap size and dielectric constant of the packing material on the plasma behaviour in a packed bed DBD reactor: a fluid modelling study *Plasma Process. Polym.* (https://doi.org/10.1002/ppap.201600129)
[20] Zhang Y, Wang H-y, Jiang W and Bogaerts A 2015 Two-dimensional particle-in cell/Monte Carlo simulations of a packed-bed dielectric barrier discharge in air at atmospheric pressure *New J. Phys.* **17** 083056
[21] Butterworth T, Elder R and Allen R 2016 Effects of particle size on CO_2 reduction and discharge characteristics in a packed bed plasma reactor *Chem. Eng. J.* **293** 55–67
[22] Manley T C 1943 The electric characteristics of the ozonator discharge *J. Electrochem. Soc.* **84** 83–96
[23] Ashpis D E, Laun M C and Griebler E L 2012 *Progress Toward Accurate Measurements of Power Consumptions of DBD Plasma Actuators* NASA/TM-2012-217449 National Aeronautics and Space Administration
[24] Reichen P, Sonnenfeld A and von Rohr P R 2011 Discharge expansion in barrier discharge arrangements at low applied voltages *Plasma Sources Sci. Technol.* **20** 055015
[25] Peeters F J J and van de Sanden M C M 2015 The influence of partial surface discharging on the electrical characterization of DBDs *Plasma Sources Sci. Technol.* **24** 015016
[26] Dou B, Bin F, Wang C, Jia Q and Li J 2013 Discharge characteristics and abatement of volatile organic compounds using plasma reactor packed with ceramic Raschig rings *J. Electrost.* **71** 939–44
[27] Tu X, Gallon H J, Twigg M V, Gorry P A and Whitehead J C 2011 Dry reforming of methane over a Ni/Al_2O_3 catalyst in a coaxial dielectric barrier discharge reactor *J. Phys. D: Appl. Phys.* **44** 274007
[28] Gómez-Ramírez A, Montoro-Damas A M, Cotrino J, Lambert R M and González-Elipe A R 2016 About the enhancement of chemical yield during the atmospheric plasma synthesis of ammonia in a ferroelectric packed bed reactor *Plasma Process. Polym.* (https://doi.org/10.1002/ppap.201600081)
[29] Pipa A V, Koskulics J, Brandenburg R and Hoder T 2012 The simplest equivalent circuit of a pulsed dielectric barrier discharge and the determination of the gas gap charge transfer *Rev. Sci. Instrum.* **83** 115112
[30] Gherardi N, Gouda G, Gat E, Ricard A and Massines F 2000 Transition from glow silent discharge to micro-discharges in nitrogen gas *Plasma Sources Sci. Technol.* **9** 340–6
[31] Peeters F J J, Rumphorst R F and van de Sanden M C M 2016 Dielectric barrier discharges revisited: the case for mobile surface charge *Plasma Sources Sci. Technol.* **25** 03LT03
[32] Kriegseis J, Grundmann S and Tropea C 2011 Power consumption, discharge capacitance and light emission as measures for thrust production of dielectric barrier discharge plasma actuators *J. Appl. Phys.* **110** 013305
[33] Kriegseis J, Möller B, Grundmann S and Tropea C 2011 Capacitance and power consumption quantification of dielectric barrier discharge (DBD) plasma actuators *J. Electrost.* **69** 302–12
[34] Ramakers M, Michielsen I, Aerts R, Meynen V and Bogaerts A 2015 Effect of argon or helium on the CO_2 conversion in a dielectric barrier discharge *Plasma Process. Polym.* **12** 755–63
[35] Whitehead J C 2016 Plasma–catalysis: the known knowns, the known unknowns and the unknown unknowns *J. Phys. D: Appl. Phys.* **49** 243001
[36] Janek J and Corte C 1999 Electrochemical blackening of yttria-stabilized zirconia—morphological instability of the moving reaction front *Solid State Ion.* **116** 181–95